Computational and Theoretical Chemistry 1080 (2016) 56–65

Contents lists available at ScienceDirect

Computational and Theoretical Chemistry

journal homepage: www.elsevier.com/locate/comptc

Conformational transition of $A\beta_{42}$ inhibited by a mimetic peptide. A molecular modeling study using QM/MM calculations and QTAIM analysis

Exequiel E. Barrera Guisasola, Lucas J. Gutiérrez, Rodrigo E. Salcedo, Francisco M. Garibotto, Sebastián A. Andujar, Ricardo D. Enriz, Ana M. Rodríguez *

Facultad de Química, Bioquímica y Farmacia, Universidad Nacional de San Luis, Chacabuco 915, 5700 San Luis, Argentina
IMIBIO-SL (CONICET), Chacabuco 915, 5700 San Luis, Argentina

ARTICLE INFO

Article history:
Received 22 December 2015
Received in revised form 2 February 2016
Accepted 2 February 2016
Available online 8 February 2016

Keywords:
Amyloid β-peptide
Mimetic peptide inhibitor
Molecular dynamics simulation
MM–GBSA analysis
ONIOM–QTAIM study

ABSTRACT

The main pathogenic event in Alzheimer's disease is believed to be the aggregation of the amyloid β-peptides into toxic aggregates. In a previous work we designed a mimetic peptide possessing a significant aggregation modulating effect by means of a molecular modeling study, using a pentameric model as a molecular target. Considerable experimental evidence indicates that oligomers as small as dimers have been involved in this disease. Therefore, an alternative therapeutic strategy might be to block the oligomerization at a monomeric level. To this end, using an $A\beta_{42}$ monomeric model, we explored the capacity and mechanism of our mimetic peptides to stabilize the α-helical conformation while preventing the formation of β-sheet structures. Long time molecular dynamics simulations and MM–GBSA analysis were coupled to investigate this issue. In addition, a combined ONIOM–QTAIM analysis was used to identify at a quantum level the most relevant interactions between $A\beta_{42}$ and this inhibitor. The computational analysis presented here pointed out six important residues of $A\beta_{42}$ (Lys16, Val36, Gly37, Gly38, Val39 and Val40) that strongly interact with our mimetic peptide, providing clues about the functional groups that might be modified in order to obtain more potent inhibitors.

1. Introduction

In the last couple of decades immeasurable hours of research and vast amounts of money have been assigned to find a solution for Alzheimer's disease (AD) without any satisfactory results. The main reason for this failure may be to disregard that this type of dementia has a multifactorial nature such as lifestyle (hypertension, diabetes, high cholesterol and smoking) and genetic background of the individual. Nevertheless, it is important to remark that the main risk factor for most forms of dementia is advanced age, with prevalence roughly doubling every five years over the age of 65 [1]. AD is an irreversible, progressive, neurodegenerative disorder characterized by the patient's memory loss and impairment of a wide range of cognitive abilities. The main neuropathological features of the disease are the accumulation of extracellular plaques composed of the amyloid-β protein (Aβ), and intracellular, hyper-phosphorylated tau forming neurofibrillary tangles and dystrophic neuritis [2].

The Aβ is derived from the amyloid precursor protein (APP) by a physiological intracellular processing that requires β- and γ-secretase activities [3]. Many alloforms with amino acid lengths varying between 39 and 43 are produced. Of these, $A\beta_{42}$ has been known to aggregate faster, and the assembled oligomers or protofibrils are more neurotoxic than other Aβ segments [4,5]. Genetic, pathologic, and biochemical evidence strongly supports the hypothesis that small-sized soluble Aβ oligomers, rather than fibrils, are the primary neurotoxic agents in AD [4,6–8]. Thus, much of the investigation has thereafter shifted from the study of fibril formation pathways toward the clarification of monomer/oligomer structural characteristics and their aggregation mechanisms.

We have recently reported the advantages and disadvantages of using a pentameric Aβ model as a molecular target for the design of new antiaggregant agents [9]. We have carried out computer simulations to study the effect of C60 on the structure and stability of a pentameric construct of Aβ units in a previous work [10]. Our investigation showed that the main effect of C60 was the destabilization of the native protofibril structure. More recently, we

* Corresponding author at: Facultad de Química, Bioquímica y Farmacia, Universidad Nacional de San Luis, Chacabuco 915, 5700 San Luis, Argentina. Tel.: +54 02664423789; fax: +54 02664431301.
E-mail address: amrodri@unsl.edu.ar (A.M. Rodríguez).

http://dx.doi.org/10.1016/j.comptc.2016.02.002
2210-271X/

performed a theoretical and experimental study of a new series of mimetic peptides possessing a significant Aβ antiaggregant/anti-oligomer effect [11]. These compounds were obtained on the basis of a molecular modeling study that allowed us to identify alterations in the structure of our $A\beta_{42}$ pentameric model [12] and quantify their effect as potential inhibitors of Aβ aggregation. Monitoring Aβ aggregation by thioflavin T fluorescence and transmission electron microscopy assays revealed that fibril formation is significantly decreased in the presence of these mimetic peptides. In addition, dot blot analysis showed a decrease of soluble oligomers strongly associated with cognitive decline in AD [13].

Experimental and theoretical investigations have indicated that during the aggregation process, the peptides first transform from their initial random coil or α-helix to β-sheet conformations and then generate oligomeric species that promote toxicity to nerve cells [14–18]. Unfortunately, the exact conformational change and molecular reorganization during this process remain to be determined. Considering that Aβ oligomers as small as dimers have been involved in AD [7], an alternative therapeutic strategy is to block oligomerization at the monomer level. With this purpose in mind, we explored in the present study the ability to and mechanism through which our mimetic peptides stabilize the helix monomeric conformation while preventing the formation of β-sheet structures. To this end, we selected the strongest antiaggregant compound from the series reported in our previous work [11] and evaluated its ability to interfere with the aggregation process, using an $A\beta_{42}$ monomeric model. In this context, stabilizing the soluble monomeric form is appealing because it can impede the formation of small oligomeric species that are recognized as the origin of neuronal damage.

Over the past few years, a growing number of theoretical studies have been conducted to analyze the Aβ monomer structures and their aggregation mechanism. Several molecular dynamics (MD) simulations have already been reported on $A\beta_{42}$ folding in aqueous solution [19–22]. In particular, replica exchange molecular dynamics (REMD) simulations, which enhance conformational sampling, have also been used [23–26]. It is worthy to remark that dissimilar results are found in many of these studies. These divergent computational conclusions on the nature of the conformations that characterize the whole ensemble of $A\beta_{42}$ monomer can be attributed to the effect of the force field and solvation model, varying extents of sampling, and to the fact that this peptide is highly disordered in solution [27]. This is the complication of intrinsically disordered proteins (also known as intrinsically unstructured), such as the $A\beta_{42}$ peptide considered here, because these systems do not populate a small number of specific conformations, but rather exist as an ensemble of rapidly interconverting structures [28]. It has been suggested that these intrinsically disordered proteins may interact with small molecules by means of specific sequence regions that exhibit specific "molecular recognition features" [29,30]. By using MD simulations combined with fragment-based drug design, it has been demonstrated that the $A\beta_{42}$ peptide in its monomeric form exhibits small molecule binding sites identified as binding hot spots [31]. The significance of these potential binding pockets was performed by docking studies of two compounds, curcumin and congo red, that have been shown to interfere the self-assembly of the Aβ peptide [32,33]. Another approach to determine the binding energy hot spots was taken by Cui et al. [34] who used residue water density and single-linkage clustering methods to predict hydrophobic regions of proteins putatively involved in binding interactions. Many additional compounds, such as other small molecules and short peptides, have been developed to stabilize Aβ in an α-helical conformation to prevent amyloid fibril formation [35–38]. Inhibitors that target residues involved in aggregation, such as Lys-specific molecular tweezers, have been shown to stabilize nontoxic Aβ oligomers by binding to Lys residues already in monomeric Aβ [39,40]. Although the discovery of these multiple compounds represents a significant progress because they can inhibit Aβ aggregation, the mechanism by which these molecules exert their effects remains somewhat unclear. Such information is crucial to the development of novel compounds capable of preventing amyloid fibril formation.

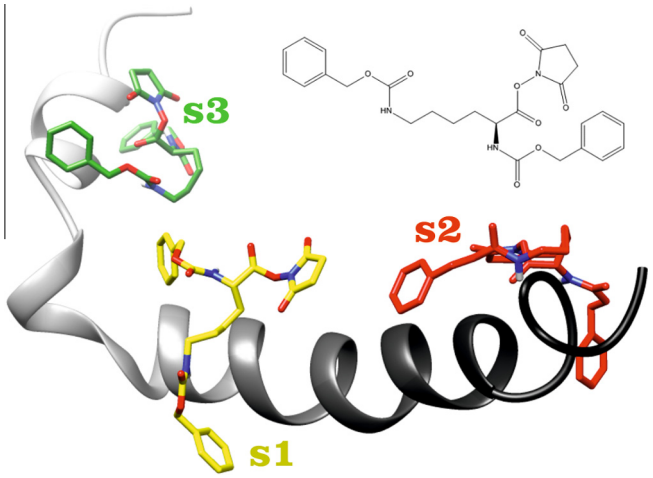

Fig. 1. Structure of DZK ligand and monomeric $A\beta_{42}$ binding sites for DZK (named s1, s2 and s3). Compound DZK is shown with different colors depending on its location at the different sites: yellow, red and green for sites 1, 2 and 3, respectively. (For interpretation of the references to colour in this figure legend, the reader is referred to the web version of this article.)

In this work, we investigated how a small mimetic peptide (*Nα*, *Nε*-Di-Z-L-lysine hydroxysuccinimide ester, DZK) interacts with monomeric $A\beta_{42}$ and prevents the conformational changes necessary for its assembly into larger sized oligomers (Fig. 1). This study is proposed based on our results obtained in dotblot analysis, using the oligomer-specific antibody A11, which showed that DZK produced an early inhibition on the formation of prefibrillar oligomers [11]. The molecular mechanism of the inhibition effect of DZK on the conformational transition of $A\beta_{42}$ was addressed by a series of long time MD simulations and the MM–GBSA method. In addition, in order to identify the most relevant interactions between $A\beta_{42}$ and this mimetic peptide, we performed more accurate quantum mechanical calculations as well as a detailed electronic analysis using the Quantum Theory of Atoms in Molecules (QTAIM) technique. To this end, we used a reduced model of the binding complex which was built taking into account the important residues of $A\beta_{42}$ discriminated according to the free energy decomposition analysis. Similar strategies have been successfully used to study other biological systems [41–44]. By using this approach, we presented evidence to understand the inhibition mechanism of DZK on the conformational transition of $A\beta_{42}$ monomeric model.

2. Computational details

2.1. Model preparation, docking setup and MD simulations

$A\beta_{42}$ monomer coordinates were taken from the Protein Data Bank (PDB entry 1IYT), which is composed of two helices [helix-1 (residues 8–25) and helix-2 (residues 28–38)] and a turn region (residues 26–27) linking the helices was used as initial structure for the MD simulations. The system was soaked in boxes of explicit water using the TIP3P model [45]. Three independent MD simulations of 50 ns were conducted under different starting velocity distribution functions. All MD simulations were performed with the Amber12 software package [46] using periodic boundary conditions and cubic simulation cells. Long-range electrostatic forces

were treated using the particle mesh Ewald method [47]. The SHAKE algorithm was applied [48] allowing for an integration time step of 2 fs. MD simulations were carried out at 310 K. The NPT ensemble was employed using Berendsen coupling to a baro/thermostat (target pressure 1 atm, relaxation time 0.1 ps). Obtained MD solutions were clustered into families using a root mean square deviation (RMSD) criterion. Program PTRAJ from the Amber12 package was employed for this type of clustering [46]. The initial $A\beta_{42}$ structure obtained from the PDB and ten conformers showing the best scores of each clustered family were submitted to a docking study. For DZK ligand, gasteiger charges were assigned and non-polar hydrogen atoms were merged. All torsions of the ligand were allowed to rotate during docking. The grid dimensions were $40 \times 40 \times 40$ points along the *x*-, *y*- and *z*-axes, with points separated by 1 Å. The grid was chosen to be sufficiently large to cover the whole system (blind docking method). The value of exhaustiveness of search was 400 and the number of poses collected was 9. All graphic manipulations and visualizations were performed by means of the AutoDock Tools 1.5.4 [49] and ligand docking was carried out *via* Autodock Vina 1.1.1. [50]. Then, representative DZK–$A\beta_{42}$ complexes were submitted to fully atomistic explicit-solvent MD simulations. The production was carried out at the NPT ensemble running 20 independent simulations with length limited to 50 ns. Each individual simulation was started reading the final coordinates obtained from the docking calculations but generating random initial velocities at the target temperature (*irest* = 0, *tempi* = 310 K) and assigning different random seeds (ig = −1). Finally, three DZK–$A\beta_{42}$ complexes and the β_{42} monomer were subjected to three more extended MD simulations (300 ns each using different starting velocity distribution functions). Secondary structure of the $A\beta_{42}$ monomer was calculated with the secstruct command using the DSSP method [51]. Spatial views shown in Figs. 1 and S1 were constructed using the UCSF Chimera program [52] as a graphic interface.

2.2. Binding free energy calculations/$A\beta_{42}$-residue interaction decomposition

The interactions between the $A\beta_{42}$ peptide and DZK ligand were calculated using the MM/GBSA decomposition method implemented in AMBER 12 [46]. The interaction between Aβ peptide–residue pairs is approximated by:

$$\Delta G_{A\beta 42\text{-residue}} = \Delta E_{vdw} + \Delta E_{ele} + \Delta G_{GB} + \Delta G_{SA} \quad (1)$$

where ΔE_{vdw} and ΔE_{ele} are respectively the non-bonded van der Waals interactions and electrostatic interactions between the Aβ peptide and each paratope residue in the gas phase. The polar contribution to solvation free energy (ΔG_{GB}) was calculated by using the GB module. ΔG_{SA} is the free energy due to the solvation process of nonpolar contribution and was calculated from SASA. All energy components in Eq. (1) were calculated using snapshots taken at 100 ps time intervals from the complete MD trajectories, removing the explicit water molecules from the snapshots.

2.3. QM/MM setup

The most important question when using the ONIOM scheme is the partitioning of the system into high and low level layers. In this work, we identified the binding site residues of the $A\beta_{42}$ monomeric model by using the free energy decomposition approach (MM/GBSA). The side chains of the binding site residues that contributed with a $|\Delta G|$ higher than 1.0 kcal/mol in the per residue energy decomposition together with DZK inhibitor were included at the high-level QM layer, and the remainder of the complex system was included in the low-level MM layer. The QM region was calculated using the B3LYP-D/6-31G(d) method [53–55] and the MM portion using the AMBER force field [56]. The MM parameters absent in the standard AMBER force field were included from the generalized amber force field (GAFF) [57]. Only the geometry of the QM layer was fully optimized. Hydrogen link atoms were used to satisfy atoms at the QM and MM interface. The hydrogen link atoms remained fixed during optimization.

2.4. Atoms in molecules theory

After the QM/MM calculation, the optimized geometry for DZK–$A\beta_{42}$ complex was used as input for QTAIM analysis [58], which was performed with the help of Multiwfn software [59], using the wave functions generated at the B3LYP-D/6-31G(d) level. This type of calculations have been used in recent works because it ensures a reasonable compromise between the wave function quality required to obtain reliable values of the derivatives of $\rho(r)$ and the computer power available, due to the extension of the system in study [42,60].

3. Results and discussion

This study was carried out in four steps. First, MD simulations were performed on different complexes of monomeric $A\beta_{42}$ with DZK, a mimetic peptide previously reported as an aggregation modulating compound [11]. In a second step, MM–GBSA free energy decomposition analysis was employed to select the residues involved in the most relevant molecular interactions of the DZK–$A\beta_{42}$ association. Then, geometric optimizations were performed using quantum mechanics and molecular mechanics (QM/MM) calculations on the DZK together with the $A\beta_{42}$ peptide. Finally, the molecular interactions were further analyzed from a QTAIM study.

3.1. MD simulations of DZK–$A\beta_{42}$ complexes

Previous experimental and theoretical studies have demonstrated that conformational conversion from the initial α-helix to β-sheet is a fundamental step in early Aβ amyloidogenesis [15,61]. To explore the inhibitory effect of DZK on the conformational transition of $A\beta_{42}$, we started our study using fully atomistic explicit-solvent MD simulations of the monomeric form in order to obtain different Aβ structures of this peptide in solution. Initially, $A\beta_{42}$ monomer (PDB-entry 1IYT) was simulated under NPT conditions for a total simulation time of 150 ns (three individual trajectories of 50 ns each). Obtained MD solutions were clustered into families using a root mean square deviation (RMSD) criterion. Program PTRAJ from the AMBER package was employed for this type of clustering [46]. Conformers showing best scores of each clustered family were promoted to docking study. Thus, ten different monomeric $A\beta_{42}$ structures were obtained and employed to explore possible DZK–$A\beta_{42}$ binding modes. For this purpose, a blind docking analysis using the program Autodock Vina was performed.

Table 1
Secondary structure analysis for the different monomeric $A\beta_{42}$ systems.[a]

	WT $A\beta_{42}$	DZK-s1-$A\beta_{42}$	DZK-s2-$A\beta_{42}$	DZK-s3-$A\beta_{42}$
Total helix[b] (%)	18.6 ± 6	28.1 ± 4	27.9 ± 12	38.4 ± 2
β-sheet[c] (%)	2.4 ± 3	2.9 ± 2	2.2 ± 1	0.5 ± 0.2
Turn (%)	25.9 ± 7	27.4 ± 4	23 ± 2	20.8 ± 1
Random coil (%)	53.1 ± 7	41.6 ± 6	46.9 ± 13	40.3 ± 3

[a] All entries reflect averages with standar deviations from three MD simulations in each set.
[b] Total helix is the sum of α-, 3_{10}-, and π-helical content.
[c] β-sheet content reflects the sum of parallel β-sheet and anti-parallel β-sheet structures.

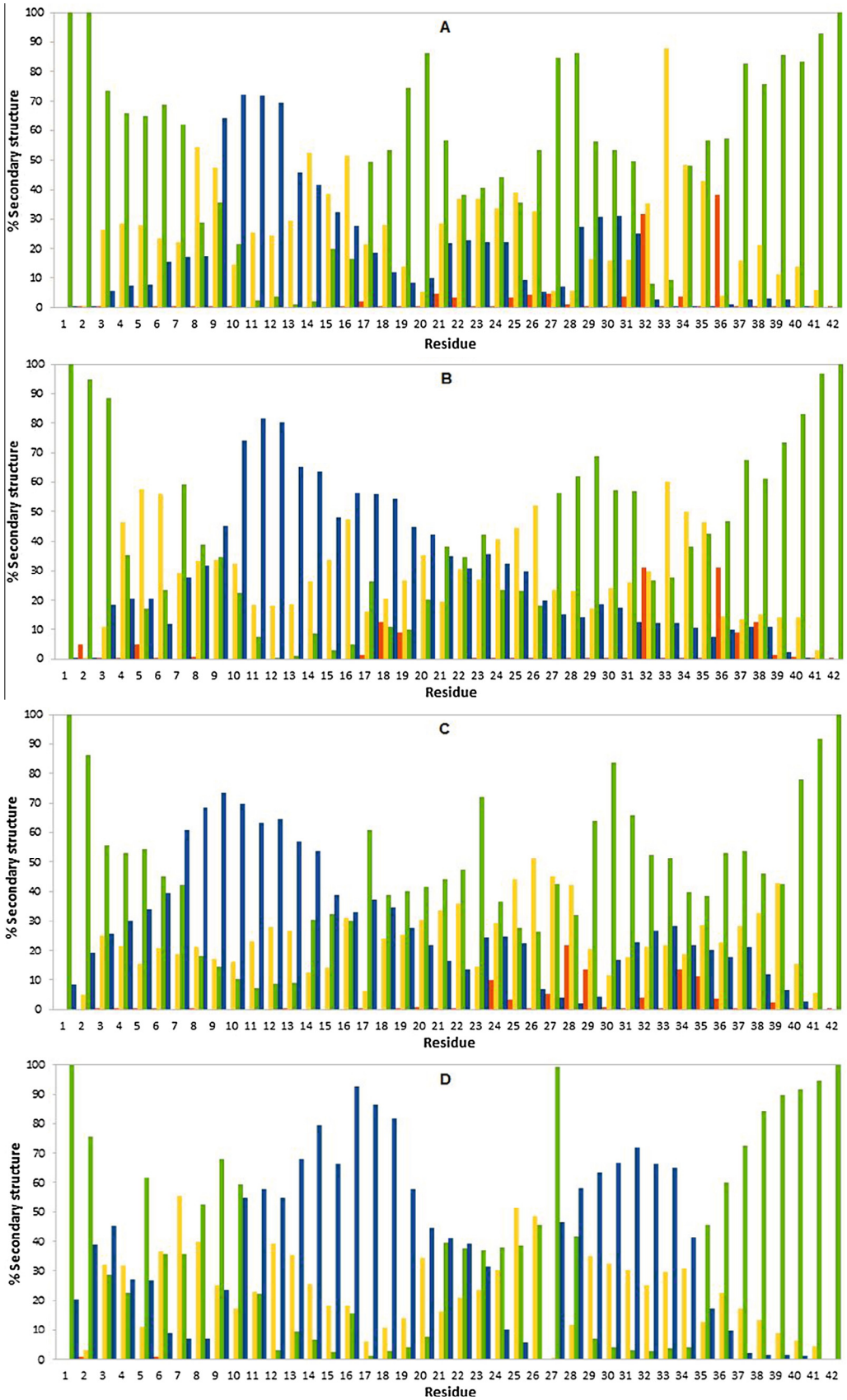

Fig. 2. Average secondary structure propensities for WT (A), DZK-s1-Aβ_{42} (B), DZK-s2-Aβ_{42} (C) and DZK-s3-Aβ_{42} (D). Random coil is shown in green, turn in yellow, helix in blue, and β-sheet in red. (For interpretation of the references to colour in this figure legend, the reader is referred to the web version of this article.)

The initial $A\beta_{42}$ structure obtained from the PDB was also submitted to the same procedure. Three main binding sites were recognized by this procedure (designated as sites s1–s3 in Fig. 1). Binding site s1 was located around the central hydrophobic cluster (CHC) region (residues Leu17–Ala21), showing the interaction of DZK with residues Phe19–Phe20 and the neighbor amino acids Lys16, Asp23, Val24 and Ile31 (site s1 in Fig. 1). The binding site s2 was located around the N-terminus residues of $A\beta_{42}$ (Asp1, Phe4, Arg5, His6, Ser8, Val12 and His13), whereas site s3 was placed at the C-terminal region of the monomer encompassing the residues Ile31, Leu34, Met35, Val39 and Ile41. These putative binding sites are in agreement with some well-defined Aβ peptide regions implicated in the amyloid fibril formation, such as the C-terminus and the sequence Lys16–Phe20 of the Aβ peptide [62,63]. In addition, a computational study on $A\beta_{42}$ monomeric model has identified small-molecules binding sites, in particular in the CHC region, which are involved in the aggregation process [31].

In the following step, twenty DZK–$A\beta_{42}$ complexes were selected and then simulated for 50 ns. This dynamic study on the different systems in solution was performed to show the ability of DZK to stabilize the helix monomeric conformation. It is important to remark that the loss of this secondary structure is observed during the conformational transition in the early stages of the formation of toxic species in Alzheimer's disease. During the simulations in the WT $A\beta_{42}$ set, much of the initial helicity of $A\beta_{42}$ was lost in favor of turn and random coil elements. In the case of DZK–$A\beta_{42}$ complexes, the helicity was generally increased showing more helical content than the control WT $A\beta_{42}$ with average percentages of 50% particularly when DZK interacts with site s1 at the CHC region (Table S1 and Fig. S1, Supplementary material).

In order to confirm the prediction of the above secondary structure analysis, three DZK–$A\beta_{42}$ complexes (DZK-s1-$A\beta_{42}$, DZK-s2-$A\beta_{42}$ and DZK-s3-$A\beta_{42}$) and the WT $A\beta_{42}$ monomer were subjected to three more extended MD simulations (300 ns each using different starting velocity distribution functions) and the corresponding results are shown in Table 1. Previous studies have shown that MD force fields have inherent limitations related to the correct balance of secondary structural elements, particularly with respect to helices [64,65]. For this reason, individual α-, π-, and 3_{10}-helical structures were summed and termed directly as total helix content. Once again, WT $A\beta_{42}$ tended to lose its helicity over the time while the binding of DZK to the peptide changes its secondary structure content since all the DZK–$A\beta_{42}$ complexes maintained more helical content than the control as shown in Table 1. While not in absolute quantitative agreement, secondary structure results obtained on WT $A\beta_{42}$ agree well with simulation results using different force fields [21,66].

The secondary structure propensities for each residue in $A\beta_{42}$ are shown in Fig. 2. WT $A\beta_{42}$ only exhibited high propensity (~70%) for helix structures in the region spanning residues Tyr10–His13 (Fig. 2A). Two more helix signals are present from Glu22 to Gly25 with a small probability of 20%, and from Gly29 to Ile32 with a propensity of 30%. All the simulations of $A\beta_{42}$ in the presence of DZK manifested higher content of helical secondary structure as well as a greater number of residues in helices conformation compared to the WT $A\beta_{42}$ (Fig. 2B–D). A longer region containing helix conformation extends from residues 4 to 39 for DZK-s1-$A\beta_{42}$ complex (Fig. 2B). In addition, at the CHC region, residues 17–21 have propensity for helical configurations of ~60%, which is higher than in WT $A\beta_{42}$ by ~30%, resulting in less random coils. DZK-s2-$A\beta_{42}$ complex is more prone than WT $A\beta_{42}$ to form helix structures at the N-terminal region at positions Ala2–Gln15 as depicted by Fig. 2C. Thus, there is a small random coil to helices transition at this region going from WT $A\beta_{42}$ to DZK-s2-$A\beta_{42}$ complex. Finally, DZK-s3-$A\beta_{42}$ complex displayed high helix signals at the CHC (~80%) and near the C-terminal (~60%) regions (Fig. 2D). Taken together, these DZK–$A\beta_{42}$ systems showed similar overall secondary structure compositions but it is in the propensity per residue that differences arise. Particularly, DZK-s1-$A\beta_{42}$ and DZK-s3-$A\beta_{42}$ complexes showed higher propensities to maintain helix structures in CHC and C-terminal regions compared to the WT $A\beta_{42}$. It is important to note these results as experimental [67] and theoretical [68] studies stated that stabilizing the helix between residues 17 and 21 (CHC) prevents the formation of oligomers larger than dimers.

In a recent work we hypothesized that DZK exerts its aggregation modulating effect preventing the formation of a toxic conformer of $A\beta_{42}$ [11]. Now, through more extensive MD simulations we analyzed the capability of DZK to inhibit the formation of this toxic turn that would bring the residue Tyr10 close to Met35 resulting in the formation of S-oxidized species, partially responsible of the intracellular ROS production [69]. From our calculations, we measured the distance between these key residues finding that WT $A\beta_{42}$ showed an average distance between Tyr10 and Met35 of 5 Å (Fig. 3). On the contrary, DZK-s1-complex maintained a distance of about 20 Å during the last 150 ns of simulation. When DZK was bound in s2 and s3 an intermediate distance was found (~10 Å). These results allowed us to assume that DZK prevents the formation of a toxic conformer in the $A\beta_{42}$ monomer.

3.2. Calculation of DZK–$A\beta_{42}$ binding energies

The MM–GBSA protocol was applied to each MD trajectory in order to calculate the relative binding energies of the DZK–$A\beta_{42}$ complexes. Binding free energies estimated for DZK to the $A\beta_{42}$ monomer at the three binding sites (sites s1–s3, Fig. 1) showed comparable values indicating that none of these binding modes might be discarded as putative binding sites.

Detailed characterization of individual energy terms of the calculated binding energies of the three DZK–$A\beta_{42}$ complexes is shown in Table 2. According to this table, nonpolar energy ($\Delta G_{nonpolar}$) is favorable for the formation of the DZK-s1-$A\beta_{42}$ complex while ΔG_{polar} is not favorable, indicating that the nonpolar interactions play a major role in the binding process. Both the van der Waals energy (ΔE_{vdw}) and nonpolar solvation term (ΔG_{SA}) were also found to be favorable for DZK binding at the site 1, but the ΔE_{vdw} term (−43.25 kcal/mol) took more than 85% of the contribution to $\Delta G_{nonpolar}$. In contrast to the nonpolar part in ΔG_{bind}, the two components of the polar free energy (ΔE_{ele} and ΔG_{GB})

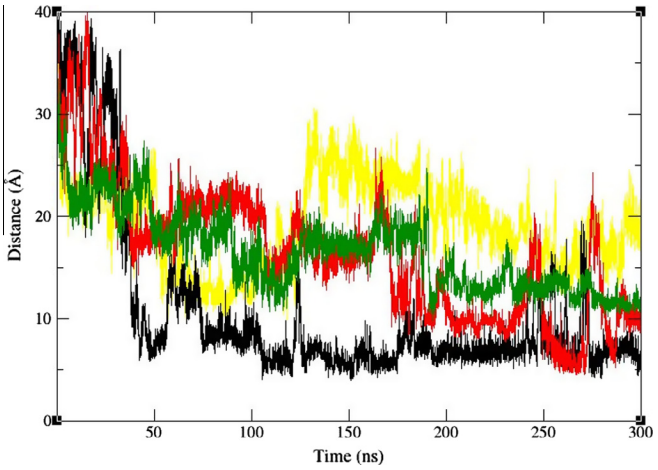

Fig. 3. Center of mass distances between residues Tyr10-Met35 for WT $A\beta_{42}$ (black), DZK-s1-$A\beta_{42}$ (yellow), DZK-s2-$A\beta_{42}$ (red) and DZK-s3-$A\beta_{42}$ (green) are shown. (For interpretation of the references to colour in this figure legend, the reader is referred to the web version of this article.)

Table 2
Binding free energy components of the DZK–Aβ_{42} complexes.

Energetic components	DZK-s1-Aβ_{42}[a]	DZK-s2-Aβ_{42}[a]	DZK-s3-Aβ_{42}[a]
ΔE_{vdw}	−43.25	−45.10	−35.13
ΔG_{SA}	−6.02	−6.13	−5.27
ΔE_{ele}	−16.73	−26.84	−15.54
ΔG_{GB}	32.52	42.25	27.63
$\Delta G_{nonpolar}$[b]	−49.27	−51.23	−40.40
ΔG_{polar}[c]	15.79	15.41	12.09
ΔG_{bind}[d]	−33.49	−35.81	−28.31

[a] Unit: kcal/mol.
[b] $\Delta G_{nonpolar} = \Delta E_{vdw} + \Delta G_{SA}$.
[c] $\Delta G_{polar} = \Delta E_{ele} + \Delta G_{GB}$.
[d] $\Delta G_{bind} = \Delta G_{nonpolar} + \Delta G_{polar}$, in which the entropy contributions of the peptide are not included.

behaved in opposite ways. Namely, the ΔE_{ele} contribution (−16.73 kcal/mol) was favorable for the binding process, while the ΔG_{GB} term (32.52 kcal/mol) greatly worked for unbinding. So, the counter-play between the two components of ΔG_{polar} disfavors the binding process. In summary, the binding free energy obtained for DZK-s1-Aβ_{42} complex was driven by favorable nonpolar interactions rather than by electrostatic interactions. It should be noted that the same behavior was observed for the binding free energy components obtained for DZK-s2-Aβ_{42} and DZK-s3-Aβ_{42} complexes (Table 2). Thus, the affinity between DZK and Aβ_{42} is dominated by hydrophobic interactions. In the following sections, these interactions will be properly analyzed evaluating the regions of Aβ_{42} peptide that might be mainly affected by DZK.

3.3. Free energy decomposition for the three DZK–Aβ_{42} complexes

The free energy decomposition not only identifies the binding energy hot spots but also gives insight into the nature of essential interactions. Hot spots refer to a handful of residues making dominant contributions to the binding process. Herein, MM–GBSA free energy decomposition analysis was also employed to select which residues of Aβ_{42} would be taken into account to define the high level layer for QM calculations. To this end, the free energy decomposition for each residue was carried out, and the results are presented in Fig. 4. The criterion of 2.5 kcal/mol was used to identify the residues having large free energy contributions. This value is the most employed in the literature [70,71]. In the DZK-s1-Aβ_{42} complex (Fig. 4A), only three residues (His13, Lys16 and Val36) made great contributions, while the other residues had a lesser

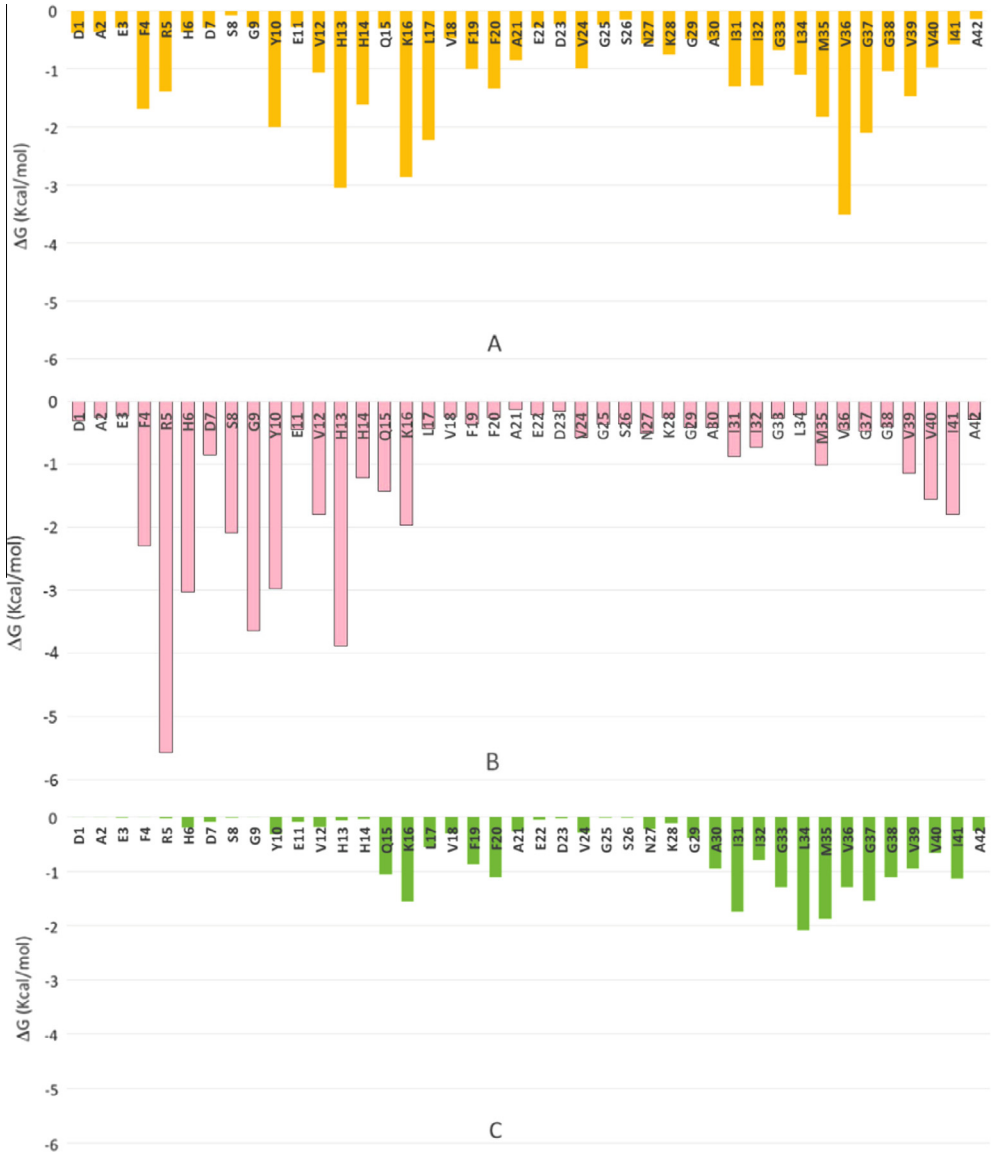

Fig. 4. Average free energy decomposition per residue of Aβ_{42} in DZK-s1-Aβ_{42} (A), DZK-s2-Aβ_{42} (B) and DZK-s3-Aβ_{42} (C).

effect. Fig. 4B shows the free energy decomposition results for the DZK-s2-Aβ_{42} complex. Five residues (Arg5, His6, Gly9, Tyr10 and His13) offer great contributions, while the remaining residues supply minor contributions. None of the residues contribute with a ΔG higher than 2.5 kcal/mol in the DZK-s3-Aβ_{42} complex (Fig. 4C).

At this point, with the purpose of identifying the most appropriate interaction site of Aβ_{42} for the QM/MM calculations, the criterion of 1 kcal/mol was used to extend the number of residues involved in the DZK–Aβ_{42} association. Thus, 18 residues of Aβ_{42} provided favorable binding free energies at the site 1 (Fig. 4A). Among them, seven residues (Phe4, Tyr10, Leu17, Phe19, Phe20, Ile31 and Met35) have been previously identified as binding hot spots that interact with each other to form favorable pockets that might be proper for binding small ligands [31]. These hot spots included residues covering N-terminal, CHC and C-terminal regions. Moreover, Lys16, reported as a key residue in Aβ fibrillogenesis [39,40], also provided a favorable binding free energy (−2.87 kcal/mol). Although binding sites 2 and 3 also showed several hot spots identified in terms of the free energy contribution of each residue, none of them covered a wide region as the binding site 1. DZK-s2-Aβ_{42} complex mainly showed great contribution of residues from the N-terminal region (Fig. 4B). Albeit DZK-s3-Aβ_{42} system displayed favorable binding free energies for residues located on the C-terminal region, this complex supplied minimal contributions on the CHC region.

In summary, DZK-s1-Aβ_{42} showed: (i) a high propensity to maintain helix structures in CHC and C-terminal regions, (ii) several hot spots covering N-terminal, CHC and C-terminal regions, including an important contribution to the free energy with Lys16, a key residue in Aβ fibrillogenesis, and (iii) an increased distance between Tyr10 and Met35, preventing the formation of the toxic turn conformer in the Aβ_{42} monomer. Taken together, these results allowed us to select the first type of complexes (indicated as site 1 in Fig. 1), where DZK is mainly bound at the CHC, to perform a quantitative analysis of the molecular interactions affecting the Aβ_{42} monomer in presence of DZK. To this end, in the following section, a combined ONIOM–QTAIM analysis was used to obtain a deep understanding of how DZK interacts with the amino acid residues of the Aβ_{42} peptide.

3.4. Evaluating the molecular interactions for the DZK–Aβ_{42} complex using QTAIM calculations

The QTAIM analysis is an important tool in the study of ligand–receptor interactions since it measures the strength of these interactions considering the values of electronic density at a bond critical point (BCP). Furthermore, this technique allows us to decompose global interactions on the contributions of each interacting functional group and thus identify which groups give the weaker interactions. These groups might be good candidates to be replaced by others that can give stronger interactions.

Accordingly, Fig. 5 shows the sum of the charge density values ($\sum\rho_{(r)}$) at the BCPs due to intermolecular interactions in DZK–Aβ_{42} complex. It is partitioned into four contributions corresponding to the core fragment (violet), R_1 (blue), R_2 (red) and R_3 substituents (green). Each category of the stacked bars indicates the anchoring strength of a different fragment of the inhibitor region; whereas the total height of the stacked bars indicates the binding strength of a residue over a given region of the monomeric Aβ_{42}.

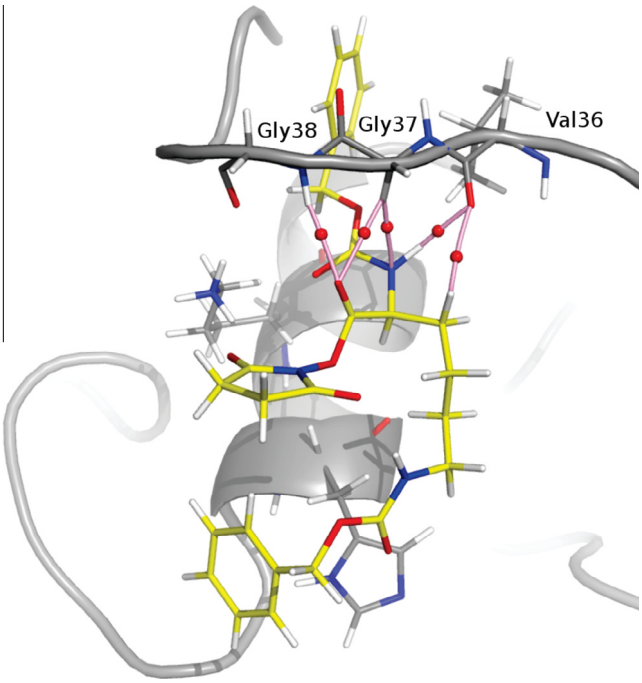

Fig. 6. Molecular graph of the non-covalent interactions between the residues Val36, Gly37, Gly38 of Aβ_{42} (gray sticks) and DZK (yellow sticks). The elements of the electron density topology are shown. The bond paths connecting the nuclei are represented in pink sticks and the bond critical points are shown as red spheres. (For interpretation of the references to colour in this figure legend, the reader is referred to the web version of this article.)

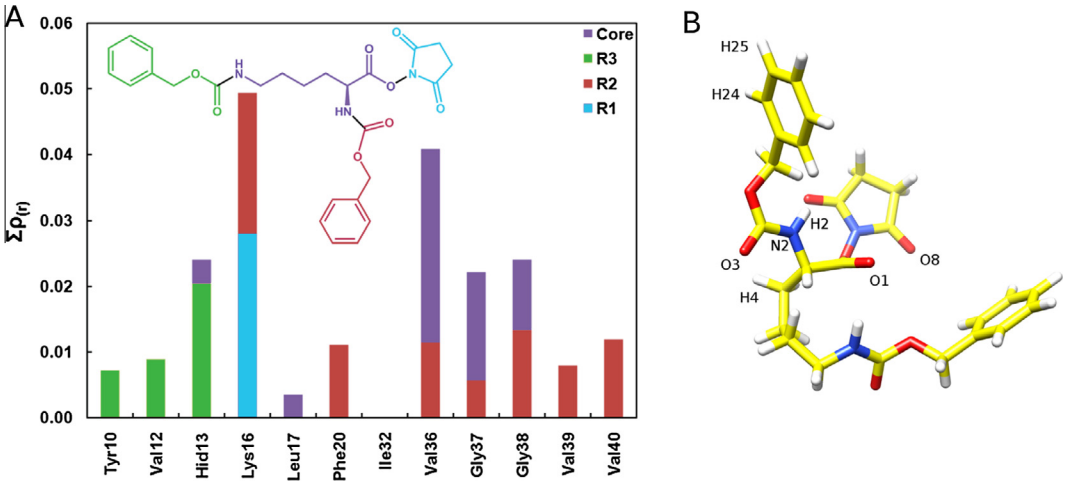

Fig. 5. (A) Sum of the charge density values ($\sum\rho_{(r)}$) at the BCPs (considering only the inter-molecular interactions) between DZK and the residues of Aβ_{42}. (B) Spatial view of DZK ligand showing the atoms that give the main interactions.

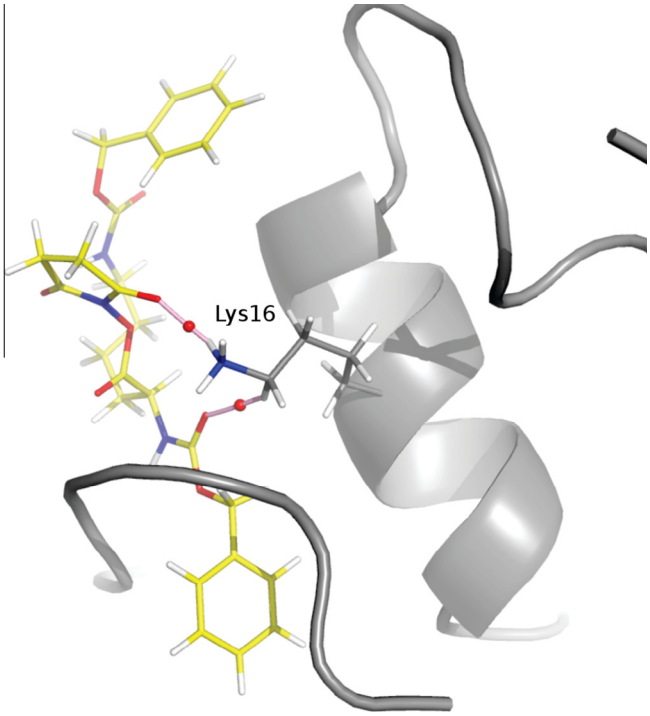

Fig. 7. Molecular graph of the non-covalent interactions between Lys16 of $A\beta_{42}$ and R_1 and R_2 groups of DZK.

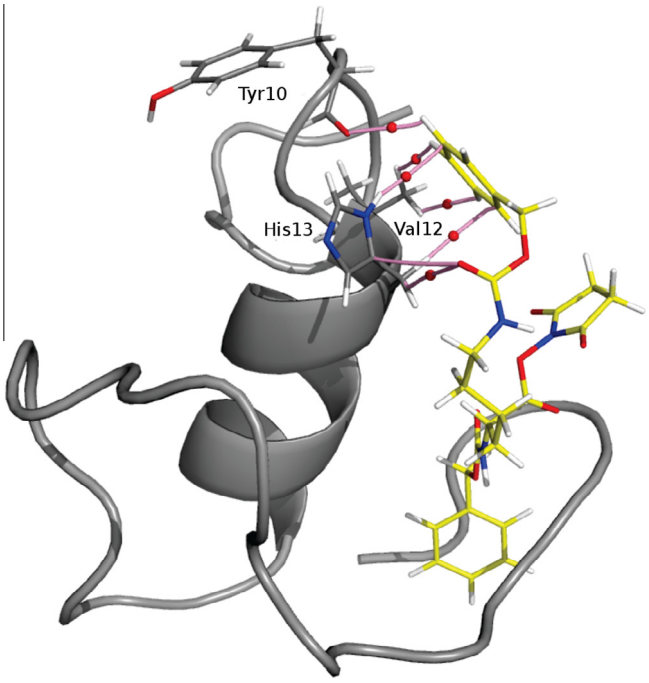

Fig. 9. Molecular graph of the non-covalent interactions between the residues Tyr10, Val12 and His13 of $A\beta_{42}$ and R_3 group of compound DZK.

As can be clearly seen in Fig. 5, the core fragment of DZK presents highest affinity to the monomer and the strongest interactions involve the residues Val36, Gly37 and Gly38, which are located in the C-terminal region. Fig. 6 displays strong H-bonds formed by the atoms H2 and H4 of DZK with the oxygen of the peptide bond of Val36 ($H2_{DZK}\cdots O_{Val36A\beta}$, $H4_{DZK}\cdots O_{Val36A\beta}$). In turn, the oxygen O1 of DZK forms strong bifurcated H-bonds with NH and HA2 atoms of Gly37 ($O1_{DZK}\cdots HA2_{Gly37A\beta}$) and Gly38 ($O1_{DZK}\cdots H_{Gly38A\beta}$), respectively. In addition, Gly37 presents a weak N···H—C interaction ($N2_{DZK}\cdots HA2_{Gly37A\beta}$). Interestingly, these interactions have also been reported for (−)-epigallocate chin-3-gallate (EGCG) in its inhibitory effect of Aβ oligomeric aggregation [72]. Moreover, the importance of a turn at Gly37–Gly38 to stabilize $A\beta_{42}$ fold and oligomers was reported previously [73], suggesting that the binding of DZK to this C-terminus region might disrupt self-assembly into quasi-spherical $A\beta_{42}$ oligomers.

The R_1 and R_2 groups are mainly involved in interactions with Lys16. Fig. 7 shows two strong interactions between Lys16 and the substituents R_1 ($O8_{DZK}\cdots HZ1_{Lys16A\beta}$) and R_2 ($O3_{DZK}\cdots HE2_{Lys16A\beta}$). This amino acid is situated adjacent to the CHC (residues 17–21), a key region in Aβ fibrillogenesis [74,75]. Lys16 has been reported to be involved in a combination of hydrophobic and electrostatic interactions which are important in initiating the aberrant self-assembly process [39,40]. Thus, DZK might alter the Aβ folding by binding to this region of monomer. This might explain, at least in part, the significant Aβ aggregation modulating activity of DZK.

The phenyl moiety present in R_2 extends deeply into the pocket formed by residues Val36, Gly37, Gly38, Val39 and Val40, making

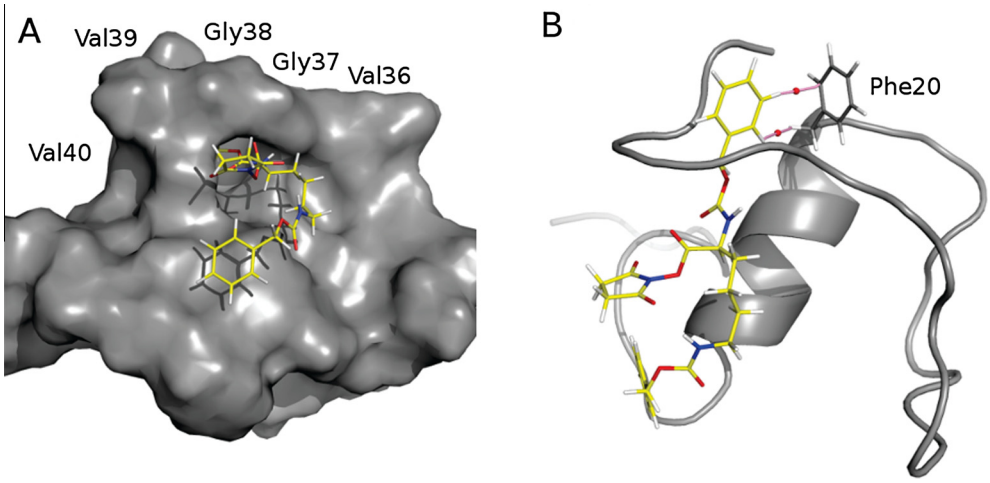

Fig. 8. (A) Spatial view of the pocket formed by residues Val36, Gly37, Gly38, Val39 and Val40 of $A\beta_{42}$ (gray surface) with DZK (yellow sticks), and (B) molecular graph of the non-covalent interactions between Phe20 of $A\beta_{42}$ and the R_2 phenyl moiety of DZK. (For interpretation of the references to colour in this figure legend, the reader is referred to the web version of this article.)

multiple favorable contacts in a cooperative way (Fig. 8A). Moreover, the edge-to-face ("T-shaped") configuration of the aromatic ring of Phe20 and the R_2 phenyl moiety of DZK favors the formation of two hydrophobic attractive contacts: $H24_{K17}\cdots CD2_{Phe20A\beta}$ and $H25_{K17}\cdots HB2_{Phe20A\beta}$ (Fig. 8B).

The R_3 substituent is located on the disordered region of the monomer which has a high mobility. Hence, interactions between the residues Tyr10, Val12, His13 and R3 group are weak (Fig. 9). As was mentioned in the first paragraph of this section, the R_3 group might be a good candidate to be replaced by a functional group which can form stronger interactions with the disordered region of the monomeric $A\beta_{42}$.

4. Conclusions

We recently reported that DZK possesses a significant $A\beta_{42}$ aggregation modulating effect [11]. The design of this compound was carried out by a molecular modeling study by using a pentameric model. Here, MD simulations, MM/GBSA analysis, QM/MM calculations and a QTAIM study were used to identify the molecular interactions of the mimetic peptide DZK with $A\beta_{42}$ in an attempt to explore how this compound stabilizes the peptide in the monomeric form and disfavors its oligomerization. Extensive MD simulations (3.6 μs) of DZK–$A\beta_{42}$ complexes showed high propensities to maintain helix structures in CHC and C-terminal regions, preventing the conformational transition of the peptide. In addition, the interaction of DZK with $A\beta_{42}$ impedes Tyr10 getting close to Met35, preventing the formation of the S-oxidized radical cation observed in the process of the toxic oligomer formation [69].

According to the results of the free energy decomposition analysis, the binding between the $A\beta_{42}$ peptide and the DZK located at binding site 1 is driven by selected "hot spots" that play a major role in DZK–$A\beta_{42}$ interactions. The most important residues are Phe4, Tyr10, Leu17, Phe19, Phe20, Ile31, and Met35, which were found to be involved in several interactions of different types, and the majority of them are supported by previous experimental and theoretical results [31,74].

The combined ONIOM–QTAIM analysis allows us to decompose the global interactions of DZK–$A\beta_{42}$ complex on the contributions of each interacting functional group. Our results indicate that the core fragment of DZK strongly interacts with the residues Val36, Gly37 and Gly38, which are located in the C-terminal region. The R1 and R2 groups are mainly involved in strong H-bonds with the residue Lys16, which plays a key role in the process of Aβ oligomerization [39,40]. In addition, the phenyl moiety present in R2 extends deeply into the pocket formed by residues Val36, Gly37, Gly38, Val39 and Val40, making several stabilizing hydrophobic contacts.

Finally, the R3 substituent of DZK, located in the disordered region of the monomer showed weak interactions. This result suggests that new and more potent mimetic peptides can be synthesized replacing the R3 group of DZK in order to optimize these interactions.

When searching compounds that might interfere at the earliest step of the amyloidogenic process, during which the monomers self-associate into toxic oligomers, such compounds should interfere with as many types of key molecular interactions as possible. In this work, we provided a detailed description of multiple molecular interactions between DZK and $A\beta_{42}$ corroborating that the computational analysis has an important role in studies of this type of disorders related with aberrant protein self-assembly. In this sense QTAIM studies are very useful to get a fairly accurate description of the strengths and weaknesses of those interactions that are important to stabilize or destabilize the molecular complexes.

Acknowledgments

Grants from Universidad Nacional de San Luis (UNSL), partially supported this work. E.E.B.G. and R.E.S. thank doctoral fellowships of CONICET-Argentina. R.D.E. and S.A.A. are members of the Consejo Nacional de Investigaciones Científicas y Técnicas (CONICET-Argentina) staff.

Appendix A. Supplementary material

Supplementary data associated with this article can be found, in the online version, at http://dx.doi.org/10.1016/j.comptc.2016.02.002.

References

[1] C. Ballard, S. Gauthier, A. Corbett, C. Brayne, D. Aarsland, E. Jones, Alzheimer's disease, Lancet 377 (2011) 1019–1031.
[2] S.A. Small, K. Duff, Linking Abeta and tau in late-onset Alzheimer's disease: a dual pathway hypothesis, Neuron 60 (2008) 534–542.
[3] D.J. Selkoe, Alzheimer's disease: genes, proteins, and therapy, Physiol. Rev. 81 (2001) 741–766.
[4] C. Haass, D.J. Selkoe, Soluble protein oligomers in neurodegeneration: lessons from the Alzheimer's amyloid beta-peptide, Nat. Rev. Mol. Cell Biol. 8 (2007) 101–112.
[5] M. Ahmed, J. Davis, D. Aucoin, T. Sato, S. Ahuja, S. Aimoto, J.I. Elliott, W.E. Van Nostrand, S.O. Smith, Structural conversion of neurotoxic amyloid-beta(1–42) oligomers to fibrils, Nat. Struct. Mol. Biol. 17 (2010) 561–567.
[6] R. Kayed, E. Head, J.L. Thompson, T.M. McIntire, S.C. Milton, C.W. Cotman, C.G. Glabe, Common structure of soluble amyloid oligomers implies common mechanism of pathogenesis, Science 300 (2003) 486–489.
[7] G.M. Shankar, S. Li, T.H. Mehta, A. Garcia-Munoz, N.E. Shepardson, I. Smith, F. M. Brett, M.A. Farrell, M.J. Rowan, C.A. Lemere, C.M. Regan, D.M. Walsh, B.L. Sabatini, D.J. Selkoe, Amyloid-beta protein dimers isolated directly from Alzheimer's brains impair synaptic plasticity and memory, Nat. Med. 14 (2008) 837–842.
[8] S.L. Bernstein, N.F. Dupuis, N.D. Lazo, T. Wyttenbach, M.M. Condron, G. Bitan, D. B. Teplow, J.-E. Shea, B.T. Ruotolo, C.V. Robinson, M.T. Bowers, Amyloid-β protein oligomerization and the importance of tetramers and dodecamers in the aetiology of Alzheimer's disease, Nat. Chem. 1 (2009) 326–331.
[9] E.E. Barrera Guisasola, L.J. Gutierrez, S.A. Andujar, E. Angelina, A.M. Rodríguez, R.D. Enriz, Pentameric models as alternative molecular targets for the design of new antiaggregant agents, Curr. Prot. Pept. Sci. 17 (2016) 156–168.
[10] S.A. Andujar, F. Lugli, S. Hofinger, R.D. Enriz, F. Zerbetto, Amyloid-β fibril disruption by C 60-molecular guidance for rational drug design, Phys. Chem. Chem. Phys. (2012) 8599–8607.
[11] E.E. Barrera Guisasola, S.A. Andujar, E. Hubin, K. Broersen, I.M. Kraan, L. Méndez, C.M.L. Delpiccolo, M.F. Masman, A.M. Rodríguez, R.D. Enriz, New mimetic peptides inhibitors of Aβ aggregation. Molecular guidance for rational drug design, Eur. J. Med. Chem. 95 (2015) 136–152.
[12] M.F. Masman, U.L.M. Eisel, I.G. Csizmadia, B. Penke, R.D. Enriz, S.J. Marrink, P.G. M. Luiten, In silico study of full-length amyloid 1–42 tri- and penta-oligomers in solution, J. Phys. Chem. B (2009) 11710–11719.
[13] M. Necula, R. Kayed, S. Milton, C.G. Glabe, Small molecule inhibitors of aggregation indicate that amyloid beta oligomerization and fibrillization pathways are independent and distinct, J. Biol. Chem. 282 (2007) 10311–10324.
[14] C. Soto, E.M. Castaño, R.A. Kumar, R.C. Beavis, B. Frangione, Fibrillogenesis of synthetic amyloid-beta peptides is dependent on their initial secondary structure, Neurosci. Lett. 200 (1995) 105–108.
[15] M.D. Kirkitadze, M.M. Condron, D.B. Teplow, Identification and characterization of key kinetic intermediates in amyloid beta-protein fibrillogenesis, J. Mol. Biol. 312 (2001) 1103–1119.
[16] W. Zhuang, N.G. Sgourakis, Z. Li, A.E. Garcia, S. Mukamel, Discriminating early stage Aβ42 monomer structures using chirality-induced 2DIR spectroscopy in a simulation study, Proc. Natl. Acad. Sci. USA (2010) 15687–15692.
[17] S. Jang, S. Shin, Amyloid beta-peptide oligomerization in silico: dimer and trimer, J. Phys. Chem. B 110 (2006) 1955–1958.
[18] G. Bellesia, J.-E. Shea, Diversity of kinetic pathways in amyloid fibril formation, J. Chem. Phys. 131 (2009) 145103–145110.
[19] D. Flöck, S. Colacino, G. Colombo, A. Di Nola, Misfolding of the amyloid beta-protein: a molecular dynamics study, Proteins 62 (2006) 183–192.
[20] E. Luttmann, G. Fels, All-atom molecular dynamics studies of the full-length β-amyloid peptides, Chem. Phys. 323 (2006) 138–147.
[21] C. Lee, S. Ham, Characterizing amyloid-beta protein misfolding from molecular dynamics simulations with explicit water, J. Comput. Chem. 32 (2011) 349–355.
[22] C. Velez-Vega, F.A. Escobedo, Characterizing the structural behavior of selected Aβ-42 monomers with different solubilities, J. Phys. Chem. B 115 (2011) 4900–4910.

[23] M. Yang, D.B. Teplow, Amyloid beta-protein monomer folding: free-energy surfaces reveal alloform-specific differences, J. Mol. Biol. 384 (2008) 450–464.
[24] S. Côté, P. Derreumaux, N. Mousseau, Distinct morphologies for amyloid beta protein monomer: Aβ 1–40, Aβ 1–42, and Aβ 1–40 (D23N), J. Chem. Theory Comput. 7 (2011) 2584–2592.
[25] N.G. Sgourakis, M. Merced-Serrano, C. Boutsidis, P. Drineas, Z. Du, C. Wang, A.E. Garcia, Atomic-level characterization of the ensemble of the Aβ(1–42) monomer in water using unbiased molecular dynamics simulations and spectral algorithms, J. Mol. Biol. 405 (2011) 570–583.
[26] A. Okamoto, A. Yano, K. Nomura, S. Higai, N. Kurita, Stable conformation of full-length amyloid-β (1–42) monomer in water: replica exchange molecular dynamics and ab initio molecular orbital simulations, Chem. Phys. Lett. 577 (2013) 131–137.
[27] J.E. Shea, B. Urbanc, Insights into Aβ aggregation: a molecular dynamics perspective, Curr. Top. Med. Chem. 12 (2012) 2596–2610.
[28] V.N. Uversky, A.K. Dunker, Understanding protein non-folding, Biochim. Biophys. Acta 2010 (1804) 1231–1264.
[29] S.J. Metallo, Intrinsically disordered proteins are potential drug targets, Curr. Opin. Chem. Biol. 14 (2010) 481–488.
[30] P. Tompa, Unstructural biology coming of age, Curr. Opin. Struct. Biol. 21 (2011) 419–425.
[31] M. Zhu, A. De Simone, D. Schenk, G. Toth, C.M. Dobson, M. Vendruscolo, Identification of small-molecule binding pockets in the soluble monomeric form of the Aβ42 peptide, J. Chem. Phys. 139 (2013) 035101.
[32] K. Ono, K. Hasegawa, H. Naiki, M. Yamada, Curcumin has potent anti-amyloidogenic effects for Alzheimer's beta-amyloid fibrils in vitro, J. Neurosci. Res. 75 (2004) 742–750.
[33] C. Lendel, B. Bolognesi, A. Wahlström, C.M. Dobson, A. Gräslund, Detergent-like interaction of Congo red with the amyloid beta peptide, Biochemistry 49 (2010) 1358–1360.
[34] D. Cui, S. Ou, S. Patel, Protein-spanning water networks and implications for prediction of protein–protein interactions mediated through hydrophobic effects, Proteins 82 (2014) 3312–3326.
[35] X.-L. Bu, P.P.N. Rao, Y.-J. Wang, Anti-amyloid aggregation activity of natural compounds: implications for Alzheimer's drug discovery, Mol. Neurobiol. (2015), http://dx.doi.org/10.1007/s12035-015-9301-4.
[36] M.J. Guerrero-Muñoz, D.L. Castillo-Carranza, R. Kayed, Therapeutic approaches against common structural features of toxic oligomers shared by multiple amyloidogenic proteins, Biochem. Pharmacol. 88 (2014) 468–478.
[37] B. Cheng, H. Gong, H. Xiao, R.B. Petersen, L. Zheng, K. Huang, Inhibiting toxic aggregation of amyloidogenic proteins: a therapeutic strategy for protein misfolding diseases, Biochim. Biophys. Acta 2013 (1830) 4860–4871.
[38] T. Liu, G. Bitan, Modulating self-assembly of amyloidogenic proteins as a therapeutic approach for neurodegenerative diseases: strategies and mechanisms, Chem. Med. Chem. 7 (2012) 359–374.
[39] S. Sinha, D.H.J. Lopes, G. Bitan, A key role for lysine residues in amyloid β-protein folding, assembly, and toxicity, ACS Chem. Neurosci. 3 (2012) 473–481.
[40] S. Sinha, D.H.J. Lopes, Z. Du, E.S. Pang, A. Shanmugam, A. Lomakin, P. Talbiersky, A. Tennstaedt, K. McDaniel, R. Bakshi, P.-Y. Kuo, M. Ehrmann, G.B. Benedek, J.A. Loo, F.-G. Klärner, T. Schrader, C. Wang, G. Bitan, Lysine-specific molecular tweezers are broad-spectrum inhibitors of assembly and toxicity of amyloid proteins, J. Am. Chem. Soc. 133 (2011) 16958–16969.
[41] E.L. Angelina, S.A. Andujar, R.D. Tosso, R.D. Enriz, N.M. Peruchena, Non-covalent interactions in receptor–ligand complexes. A study based on the electron charge density, J. Phys. Org. Chem. 27 (2014) 128–134.
[42] R.D. Tosso, S.A. Andujar, L. Gutierrez, E. Angelina, R. Rodríguez, M. Nogueras, H. Baldoni, F.D. Suvire, J. Cobo, R.D. Enriz, Molecular modeling study of dihydrofolate reductase inhibitors. Molecular dynamics simulations, quantum mechanical calculations, and experimental corroboration, J. Chem. Inf. Model. 53 (2013) 2018–2032.
[43] J. Párraga, N. Cabedo, S. Andujar, L. Piqueras, L. Moreno, A. Galán, E. Angelina, R. D. Enriz, M.D. Ivorra, M.J. Sanz, D. Cortes, 2,3,9- and 2,3,11-Trisubstituted tetrahydroprotoberberines as D2 dopaminergic ligands, Eur. J. Med. Chem. 68 (2013) 150–166.
[44] S. Boopathi, P. Kolandaivel, Study on the inter- and intra-peptide salt-bridge mechanism of Aβ23-28 oligomer interaction with small molecules: QM/MM method, Mol. BioSyst. 11 (2015) 2031–2041.
[45] W.L. Jorgensen, J. Chandrasekhar, J.D. Madura, R.W. Impey, M.L. Klein, Comparison of simple potential functions for simulating liquid water, J. Chem. Phys. 79 (1983) 926–935.
[46] D.A. Case, T.E. Cheatham, T. Darden, H. Gohlke, R. Luo, K.M. Merz, A. Onufriev, C. Simmerling, B. Wang, R.J. Woods, The Amber biomolecular simulation programs, J. Comput. Chem. 26 (2005) 1668–1688.
[47] U. Essmann, L. Perera, M.L. Berkowitz, T. Darden, H. Lee, L.G. Pedersen, A smooth particle mesh Ewald method, J. Chem. Phys. 103 (1995) 8577–8593.
[48] J.-P. Ryckaert, G. Ciccotti, H.J. Berendsen, Numerical integration of the Cartesian equations of motion of a system with constraints: molecular dynamics of n-alkanes, J. Comput. Phys. 23 (1977) 327–341.
[49] M.F. Sanner, Python: a programming language for software integration and development, J. Mol. Graph. Model. 17 (1999) 57–61.
[50] O. Trott, A.J. Olson, AutoDock Vina: improving the speed and accuracy of docking with a new scoring function, efficient optimization, and multithreading, J. Comput. Chem. 31 (2010) 455–461.
[51] W. Kabsch, C. Sander, Dictionary of protein secondary structure: pattern recognition of hydrogen-bonded and geometrical features, Biopolymers 22 (1983) 2577–2637.
[52] E.F. Pettersen, T.D. Goddard, C.C. Huang, G.S. Couch, D.M. Greenblatt, E.C. Meng, T.E. Ferrin, UCSF Chimera–a visualization system for exploratory research and analysis, J. Comput. Chem. 25 (2004) 1605–1612.
[53] A. Becke, Density-functional exchange-energy approximation with correct asymptotic behavior, Phys. Rev. A 38 (1988) 3098–3100.
[54] C. Lee, W. Yang, R. Parr, Development of the Colle–Salvetti correlation-energy formula into a functional of the electron density, Phys. Rev. B: Condens. Matter 37 (1988) 785–789.
[55] S. Grimme, Semiempirical GGA-type density functional constructed with a long-range dispersion correction, J. Comput. Chem. 27 (2006) 1787–1799.
[56] W.D. Cornell, P. Cieplak, C.I. Bayly, I.R. Gould, K.M. Merz, D.M. Ferguson, D.C. Spellmeyer, T. Fox, J.W. Caldwell, P.A. Kollman, A second generation force field for the simulation of proteins, nucleic acids, and organic molecules, J. Am. Chem. Soc. 117 (1995) 5179–5197.
[57] J. Wang, R.M. Wolf, J.W. Caldwell, P.A. Kollman, D.A. Case, Development and testing of a general amber force field, J. Comput. Chem. 25 (2004) 1157–1174.
[58] R.F.W. Bader, Atoms in molecules, Acc. Chem. Res. 18 (1985) 9–15.
[59] T. Lu, F. Chen, Multiwfn: a multifunctional wavefunction analyzer, J. Comput. Chem. 33 (2012) 580–592.
[60] E.G. Vega-Hissi, R. Tosso, R.D. Enriz, L.J. Gutierrez, Molecular insight into the interaction mechanisms of amino-2 H-imidazole derivatives with BACE1 protease: a QM/MM and QTAIM study, Int. J. Quantum Chem. 115 (2015) 389–397.
[61] N. Cerdà-Costa, A. Esteras-Chopo, F.X. Avilés, L. Serrano, V. Villegas, Early kinetics of amyloid fibril formation reveals conformational reorganisation of initial aggregates, J. Mol. Biol. 366 (2007) 1351–1363.
[62] M.Q. Liao, Y.J. Tzeng, L.Y.X. Chang, H.B. Huang, T.H. Lin, C.L. Chyan, Y.C. Chen, The correlation between neurotoxicity, aggregative ability and secondary structure studied by sequence truncated Aβ peptides, FEBS Lett. 581 (2007) 1161–1165.
[63] L.O. Tjernberg, C. Lilliehöök, D.J. Callaway, J. Näslund, S. Hahne, J. Thyberg, L. Terenius, C. Nordstedt, Controlling amyloid beta-peptide fibril formation with protease-stable ligands, J. Biol. Chem. 272 (1997) 12601–12605.
[64] D. Matthes, B.L. de Groot, Secondary structure propensities in peptide folding simulations: a systematic comparison of molecular mechanics interaction schemes, Biophys. J. 97 (2009) 599–608.
[65] E.J. Sorin, V.S. Pande, Exploring the helix-coil transition via all-atom equilibrium ensemble simulations, Biophys. J. 88 (2005) 2472–2493.
[66] J.A. Lemkul, D.R. Bevan, Morin inhibits the early stages of amyloid β-peptide aggregation by altering tertiary and quaternary interactions to produce "off-pathway" structures, Biochemistry 51 (2012) 5990–6009.
[67] A. Kapurniotu, A. Buck, M. Weber, A. Schmauder, T. Hirsch, J. Bernhagen, M. Tatarek-Nossol, Conformational restriction via cyclization in β-amyloid peptide Aβ(1–28) leads to an inhibitor of Aβ(1–28) amyloidogenesis and cytotoxicity, Chem. Biol. 10 (2003) 149–159.
[68] A.V. Rojas, A. Liwo, H.A. Scheraga, A study of the α-helical intermediate preceding the aggregation of the amino-terminal fragment of the β amyloid peptide (Aβ(1–28)), J. Phys. Chem. B 115 (2011) 12978–12983.
[69] K. Murakami, K. Irie, H. Ohigashi, H. Hara, M. Nagao, T. Shimizu, T. Shirasawa, Formation and stabilization model of the 42-mer Abeta radical: implications for the long-lasting oxidative stress in Alzheimer's disease, J. Am. Chem. Soc. 127 (2005). 15168–1574.
[70] B. Huang, F.-F. Liu, X.-Y. Dong, Y. Sun, Molecular mechanism of the affinity interactions between protein A and human immunoglobulin G1 revealed by molecular simulations, J. Phys. Chem. B 115 (2011) 4168–4176.
[71] V. Lafont, M. Schaefer, R.H. Stote, D. Altschuh, A. Dejaegere, Protein–protein recognition and interaction hot spots in an antigen-antibody complex: free energy decomposition identifies "efficient amino acids", Proteins 67 (2007) 418–434.
[72] F.-F. Liu, X.-Y. Dong, L. He, A.P.J. Middelberg, Y. Sun, Molecular insight into conformational transition of amyloid β-peptide 42 inhibited by (−)-epigallocatechin-3-gallate probed by molecular simulations, J. Phys. Chem. B 115 (2011) 11879–11887.
[73] B. Urbanc, L. Cruz, S. Yun, S.V. Buldyrev, G. Bitan, D.B. Teplow, H.E. Stanley, In silico study of amyloid β-protein folding and oligomerization, PNAS 101 (2004) 17345–17350.
[74] W.P. Esler, E.R. Stimson, J.R. Ghilardi, Y.A. Lu, A.M. Felix, H.V. Vinters, P.W. Mantyh, J.P. Lee, J.E. Maggio, Point substitution in the central hydrophobic cluster of a human beta-amyloid congener disrupts peptide folding and abolishes plaque competence, Biochemistry 35 (1996) 13914–13921.
[75] N.S. de Groot, F.X. Aviles, J. Vendrell, S. Ventura, Mutagenesis of the central hydrophobic cluster in Abeta42 Alzheimer's peptide. Side-chain properties correlate with aggregation propensities, FEBS J. 273 (2006) 658–668.